Enthalpy Relaxation in Polymers: A Comparison among Different Multiparameter Approaches Extending the TNM/AGV Model

Laura Andreozzi,* Massimo Faetti, Marco Giordano, Diego Palazzuoli, and Fabio Zulli

Department of Physics "E. Fermi", University of Pisa and INFM UdR Pisa, via Buonarroti 2, I-56127 Pisa, Italy

Received June 10, 2003; Revised Manuscript Received July 10, 2003

ABSTRACT: The enthalpy recovery mechanism of polymers is usually described in terms of the Tool−Narayanaswamy−Moynihan model (TNM). Even if it is able to qualitatively reproduce all the peculiar features of the aging process, clear discrepancies have been found in quantitative analysis. In this work, differential scanning calorimetry experiments are performed in two different polymers, and data are used in order to compare the predictions of a recently developed configurational approach with possible extensions of the TNM model. All the approaches add a free parameter with respect to the original TNM model. In this study we have found that appreciable improvements between experimental and calculated DSC traces can be observed if the configurational entropy approach is adopted. Furthermore, the long-term annealing experiments performed in one of the polymers clearly support the basic hypothesis of the entropic approach concerning the limit state of the structural relaxation.

1. Introduction

Physical aging, or structural relaxation, of polymers and glasses has been intensively studied in the past years by means of many different experimental techniques such as differential scanning calorimetry (DSC), dielectric spectroscopy, dynamical mechanical analysis, dilatometry, Brillouin scattering, and so on.[1−3] This process characterizes glass-forming materials and turns out to be very important from both a fundamental and a practical point of view. In fact, it is strictly related to the glass transition, a phenomenon still poorly understood, and it can also strongly affect physical properties of polymers at long times. The latter feature acquires great importance in applicative potentialities of these materials. All these facts make desirable theoretical models with good predictive power.

Some peculiarities of the structural relaxation are presently well established from an experimental point of view. The most important ones are its nonexponential character, leading to the memory effect,[1,4,5] and nonlinearity, the latter evidenced by the asymmetry in approaching equilibrium after upward or downward temperature jumps.[1,4,5] Several phenomenological and molecular approaches have been proposed in the past,[4−8] but a thoroughly satisfactory model is still lacking. One of the most used approaches was developed several years ago by Narayanaswamy and Moynihan,[4,9−11] where the concept of fictive temperature, originally introduced by Tool,[12] was employed to deal with nonlinearity. This approach, usually in the literature referred to as the TNM model, has been mainly tested in dilatometric and calorimetric experiments, probing volume and enthalpy relaxation, respectively. In particular, calorimetric experiments with differential scanning calorimetry represent a severe test for this model. In fact, this technique allows one to record the temperature dependence of the heat capacity ($C_p(T)$) during a heating scan after a thermal history which can also reach great complexity, and that usually involves cooling at a fixed rate and aging in the glass. Because of the structural relaxation that occurred during the annealing, the enthalpy recovers its equilibrium value in the subsequent heating scan near the glass transition temperature. The process manifests itself as a peak observed in the $C_p(T)$ trace. The position and the shape of this peak, overshooting the glass transition, are strongly dependent on the details of the annealing procedure. In general, the TNM model is able to accurately reproduce the observed shape of the $C_p(T)$ curve after a given thermal history and to give an account of the material memory effects. However, especially in polymers, incompatibilities among predictions for different DSC scans have been observed.[4,13,14] In fact, the model parameters obtained by fitting the experimental thermograms pertaining to different thermal histories are often quite different, at variance with their model interpretation as material parameters. Furthermore, different experimental studies suggested that the enthalpy, lost after aging the samples in the glass for long times, was largely overestimated by the model predictions.[14,15] These difficulties cannot be entirely ascribed to the experimental errors as shown by literature studies.[4,16,17] This leads one to think that some of the main assumptions of the TNM model should be reconsidered. Several arguments suggest that the observed difficulties could be related to the way in which nonlinearity is introduced in the model through the fictive temperature.[18] Gómez Ribelles and co-workers recently have developed a configurational entropy approach that extends somewhat the TNM model and improves the agreement with DSC experiments in several polymers;[19−21] however, the model introduces an additional free parameter. In this work we compare the predictive power of the above configurational entropy model with different modifications of the TNM formalism which also add a free parameter. We test the different approaches by using DSC experiments carried out in two different polymers. One of them is a commercial poly(methyl methacrylate), whereas the other

* Corresponding author: e-mail laura.andreozzi@df.unipi.it; Fax +39 050 2214890; phone +39 050 2214891.

10.1021/ma0347870 CCC: $25.00
Published on Web 08/19/2003

is a photosensitive side-chain liquid crystal copolymer. In the next section the models are briefly described.

2. Theoretical Section

The TNM model is based on fundamental assumptions[4,5,9−11] briefly reviewed in the following. The nonexponentiality of the relaxation is described by the stretched exponential function:

$$\Phi(t) = \exp\left[-\left(\frac{t}{\tau}\right)^{\beta}\right] \tag{1}$$

with the stretching parameter β ($0 < \beta \leq 1$) which determines the broadness of the relaxation time spectrum. This latter is considered constant by invoking the time temperature superposition principle. To take into account the nonlinearity, the instantaneous relaxation times are assumed to depend on both temperature and structure. Following the idea of Tool,[12] a fictive temperature T_f is defined as a structural parameter. If the enthalpy H is taken as the relevant observable, T_f may be defined by[4]

$$H(T) = H_{eq}(T_f) - \int_T^{T_f} C_p^{glass}(\theta)\, d\theta \tag{2}$$

where C_p^{glass} is the unrelaxed glassy heat capacity. This definition implies a fundamental assumption of the model, namely, that the equilibrium values of the thermodynamic variables in the glassy state are obtained by extrapolating the equilibrium liquid or rubbery curves below the glass transition temperature ($dH_{eq}(T)/dT = C_p^{liq}(T)$).

The model also assumes that the reduced time $\xi(t) = \int 1/[\tau(T(t),T_f(t))]\, dt$ restores linearity so that the Boltzmann superposition principle can be used in order to describe the response to multiple temperature perturbation steps. It is obtained:

$$T_f(T) = T_0 + \int_{T_0}^{T}\left\{1 - \exp\left[-\left(\int_{T'}^{T}\frac{dT''}{Q\tau(T_f, T'')}\right)^{\beta}\right]\right\} dT' \tag{3}$$

T_0 is a reference temperature well above the glass transition temperature and $Q = Q_{c,h}$ represents the cooling/heating rate. By numerically integrating eq 3, the normalized heat capacity (dT_f/dT) may be evaluated and compared with the experimental value obtained by differentiating eq 2:

$$\frac{dT_f}{dT} = \frac{C_p(T) - C_p^{glass}(T)}{\Delta C_p(T_f)} \approx \frac{C_p(T) - C_p^{glass}(T)}{\Delta C_p(T)} \equiv C_p^N(T) \tag{4}$$

where $\Delta C_p(T) = C_p^{liq}(T) - C_p^{glass}(T)$ is the heat capacity increment between the glassy and liquid state. The model is then completed by choosing a specific expression for the relaxation times $\tau(T,T_f)$. The original relation proposed by Narayanaswamy and Moynihan[9−11] was the empirical modified Arrhenius expression:

$$\tau(T_f,T) = A\exp\left[\frac{x\Delta h}{RT} + \frac{(1-x)\Delta h}{RT_f}\right] \tag{5}$$

where the parameter x ($0 \leq x \leq 1$) separates the thermodynamic and the structural contribution to the relaxation times. Because the shape of the calculated annealing peaks is strongly dependent on the behavior of the out of equilibrium relaxation times, the handling of nonlinearity through the relation $\tau(T,T_f)$ should play a major role as far as the difficulty is concerned in reproducing different thermograms with the same set of parameters. Years ago, Scherer[22] and Hodge[23] proposed a different expression for $\tau(T,T_f)$, which can be derived, after some ad hoc assumptions, by extending to the out of equilibrium case the Adam−Gibbs theory:[24]

$$\tau(T_f,T) = A\exp\left[\frac{B}{RT\left(1 - \frac{T_2}{T_f}\right)}\right] \tag{6}$$

In this expression nonlinearity is mainly driven by the Adam−Gibbs temperature T_2; in fact, a correlation between T_2 and x parameter of eq 5 can be developed.[23,25] When eq 6 is used, this formalism is referred to as the AGV model because of the additional hypotheses. Even if this expression seems to be physically more robust than eq 5, it has been often found that they are quite similar regarding the predictive power of the model.[4] In particular, the difficulty met in the simultaneous reproduction of several thermograms is not removed by using eq 6. A different approach has been recently developed by Gómez Ribelles and coworkers.[19−21] The configurational entropy is adopted as structural parameter, and an evolution equation is proposed which is very similar in form to the constitutive equation of the TNM model:

$$S_c(t) = S_c^{eq}(T_0) + \int_{T_0}^{T(t)}\frac{\Delta C_p^{lim}(\theta)}{\theta}\, d\theta - \sum_{i=1}^{n}\int_{T_{i-1}}^{T_i}\frac{\Delta C_p^{lim}(\theta)}{\theta} d\theta \exp\left[-\left(\int_{t_{i-1}}^{t_i}\frac{d\lambda}{\tau(\lambda)}\right)^{\beta}\right] \tag{7}$$

where T_0 is a reference temperature above the glass transition and S_c^{eq} the equilibrium configurational entropy:

$$S_c^{eq}(T) = \int_{T_2}^{T}\frac{\Delta C_p(\theta)}{\theta}\, d\theta \tag{8}$$

In eq 8, T_2 plays the role of the Kauzmann temperature.[26] The out of equilibrium relaxation times are again defined by an extension of the Adam−Gibbs theory:

$$\tau(t) = \tau(S_c(t),\, T(t)) = A\exp\left(\frac{B}{S_c T}\right) \tag{9}$$

The main difference with the AGV model is represented by the fact that, in eq 7, the term $\Delta C_p^{lim}(T) = C_p^{lim}(T) - C_p^{glass}(T)$ appears instead of in principle expected $\Delta C_p(T)$. This means that, with this formalism, the assumption that the limit value of configurational heat capacity in the glass (and then entropy and enthalpy) is obtained by an extrapolation procedure from the melt ($C_p^{lim}(T) = C_p^{liq}(T)$ for $T < T_g$) becomes unnecessary; in this way other possibilities can be tested. To compare theoretical predictions and DSC experiments, an identical relaxation mechanism for configurational entropy and enthalpy is invoked:

$$H_c(T) = H_c^{lim}(T) - \sum_{i=1}^{n} \int_{T_{i-1}}^{T_i} \Delta C_p^{lim}(\theta)\, d\theta \exp\left[-\left(\int_{t_{i-1}}^{t_i} \frac{d\lambda}{\tau(\lambda)}\right)^{\beta}\right] \quad (10)$$

so that the theoretical $C_p(T)$ curves can be obtained from the relationship

$$C_p(T) - C_p^{glass}(T) = \frac{\partial H_c}{\partial T} \quad (11)$$

However, because information on the temperature dependence of $C_p^{lim}(T)$ is lacking, additional assumptions are necessary. To take into account the overestimation often observed for the enthalpy lost on aging the samples in the glass, the authors introduced a phenomenological shift δ of the $C_p^{lim}(T)$ with respect to $C_p^{liq}(T)$ in a narrow temperature range around the glass transition temperature.[20] This schematization is shown in Figure 1, where the corresponding behavior of the configurational entropy is also sketched.

In this way the nonlinearity degree introduced in the model is also related to the value of the additional parameter δ. This model improved the agreement with the experimental scans in simultaneous fitting procedures for several polymers.[20,21,27] This could have been expected in principle because the entropic model extends the AGV approach by adding one free parameter. To give physical support to this approach, it is worthwhile to compare it with other possible modifications of TNM model that also add one parameter and change the treatment of nonlinearity. To start with, one could consider the reasons leading to the similarity of TNM and AGV models in fitting DSC experiments. This is mainly due to the common prediction that, over a small range of temperature around the glass transition, the ratio of the nonlinear to the linear relaxation time at a given temperature, $\tau/\tau_{eq} = \tau(T,\ T \neq T_f)/\tau(T,\ T = T_f)$, depends to a good approximation only on the difference $(T - T_f)$.[18] In fact, from eqs 5 and 6 it is easily obtained:

$$\ln\left(\frac{\tau}{\tau_{eq}}\right) = (1 - x)\frac{\Delta h}{RTT_f}(T - T_f) \quad (12)$$

$$\ln\left(\frac{\tau}{\tau_{eq}}\right) = \frac{BT_2}{RT(T - T_2)(T_f - T_2)}(T - T_f) \quad (13)$$

It could be argued that terms of higher order in $(T - T_f)$ than linear provide an improvement in fitting experimental data. There is an experimental finding supporting this hypothesis. It deals with the enthalpy $\Delta H(T_a,t_a)$ lost on aging a polymer at a given temperature T_a in the glass for a time t_a, that shows a linear dependence on log t_a in a wide range of annealing times. This allows one to define a relaxation rate $R_H(T_a) = d\Delta H(T_a,t_a)/d \log t_a$, which is a function of the annealing temperature. Malek[28,29] found an analytical expression providing $R_H(T_a)$ in terms of the TNM or AGV parameters. Analyzing a large amount of experimental data, he found in several polymers systematic discrepancies between theory and experiments for a large departure from equilibrium (typically $T_g - T_a \geq 10$ K). He was able to show that the addition of a quadratic term in the NM expression

$$\tau(T_f,T) = A \exp\left[\frac{x\Delta h}{RT} + \frac{(1 - x)\Delta h}{RT_f} - k(T - T_f)^2\right] \quad (14)$$

with k of the order of 10^{-2}–10^{-3}, provided a good description of experiments also at large $T_g - T_a$.[29] In this work we take into consideration eq 14 to fit experimental DSC thermograms.

Alternatively a more general, but empirical, dependence of $\ln(\tau/\tau_{eq})$ on $T - T_f$ should be considered. Moynihan,[18] for example, suggested the power law $\ln(\tau/\tau_{eq}) = C(T - T_f)^m$. Starting from this hint and eq 13, we put

$$\ln(\tau/\tau_{eq}) = \text{sign}(T - T_f)\left[\frac{BT_2}{RT(T - T_2)(T_f - T_2)}\right](|T - T_f|)^m \quad (15)$$

with τ_{eq} given by eq 6 ($T_f = T$). In eq 15, sign$(T - T_f)$ means 1 if $T > T_f$ and -1 if $T < T_f$. As a final equation, we consider the phenomenological expression

$$\tau = A\left(\frac{T_f - T_c}{T_c}\right)^{-\gamma} \exp\left(k\frac{T_f}{T}\right) \quad (16)$$

The above expression brings, at the equilibrium, to the scaling law $\tau_{eq} = C(T - T_c)^{-\gamma}$ that, according to a recent paper,[30] fits relaxation experiments in supercooled fluids better than the Vogel–Fulcher law when $T_c < T_g$. It is worth noting that the same scaling law is predicted by the mode coupling theory,[31] even if it provides values for the critical temperature considerably higher than T_g. On the contrary, when in the deeply glassy state T_f becomes almost constant, eq 16 predicts an Arrhenius behavior such as the TNM or AGV expressions. It should be emphasized that the last expression proposed has empirical character, and it is not derived in the framework of a theoretical tool.

3. Experimental Procedure

The side-chain liquid crystal copolymer was obtained by adding 20% of standard MMA monomers to a methacrylate monomer containing a (3-methyl-4′-pentyloxy)azobenzene mesogenic unit connected at the 4-position by an hexamethylene spacer to the main chain. This random copolymer has been synthesized following a general literature procedure.[32] X-ray measurements have confirmed its nematic character in the temperature range between the glass transition T_g and the clearing temperature T_i. The value of T_g, determined according to the enthalpic definition[33] for a cooling rate of 40 K/min, is 308 K, whereas its clearing temperature is $T_i = 348$ K. The copolymer exhibits $M_n \approx 8000$ g/mol and $M_w \approx 31\,000$ g/mol. The PMMA polymer was purchased from Labservice Analytica and used as received without any further purification. Its weight-average molecular weight was $M_w \approx 21\,000$ g/mol, and the sample was almost monodisperse ($M_w/M_n = 1.07$), with glass transition temperature $T_g = 392$ K.

Differential scanning calorimetry measurements were carried out with a Perkin-Elmer DSC 7 frequently calibrated with indium and zinc standards. Highly pure nitrogen was used as a purge gas. For each polymer a single sample of about 10 mg was used for all the measurements. The experimental procedure was as follows: the sample was maintained at high temperature for some minutes in order to erase any previous treatment. Then it was cooled at $Q_c = 40$ K/min to the selected annealing temperature T_a, where it was annealed for a time t_a. It was then cooled again ($Q_c = 40$ K/min) to the starting temperature ($T_g - 80$ K) of the themograms and successively heated at 10 K/min to record the signal. After each experiment, a reference scan (cooling/heating with rates 40 and 10 K/min, respectively) was immediately recorded to evaluate the enthalpy loss due to aging (see next section).

4. Results and Discussion

To test and compare the different approaches previously described, we have employed simultaneous fitting

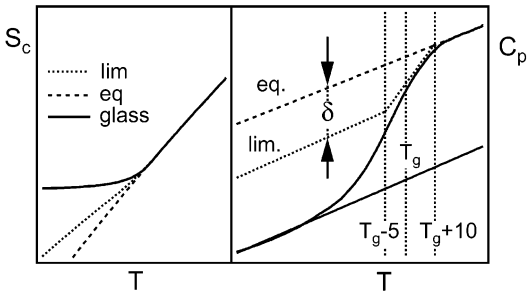

Figure 1. Scheme of the phenomenological parameter δ introduced in the configurational entropy model representing the shift in the limit glassy heat capacity with respect to its extrapolation from the melt (right). On the left, the δ effects on the configurational entropy are shown.

procedures, with the aim of reproducing six different experimental scans with a single set of parameters. The Nedler−Mead search routine[34] was used to find the best parameters by minimizing a weighted total square deviation:

$$SS = \frac{1}{6N}\sum_{i=1}^{6}\sum_{j=1}^{N} w(i)^2 (C^N_{p_{exp}}(i,j) - C^N_{p_{theory}}(i,j))^2 \quad (17)$$

In this expression the index i identifies the experimental scan, whereas the index j identifies the different points in each scan; $w(i)$ is the weight factor. Because of the strong correlation among the parameters defining the different models,[23,35] one of them was kept fixed during the fitting, whereas the others were changed by the search routine. For example, in the case of TNM model, we performed the fitting procedure for several fixed values of the activation energy Δh of eq 5.

It is worth to note that, in the literature, methods for independent evaluations of some of the model parameters can be found.[4] As an example, the value of the activation energy Δh (eq 5) can be obtained via the cooling rate dependence of T_g.[4] However, this procedure often leads to Δh values which do not minimize the square deviation of the fitting procedure. The main task of the present work being a consistent comparison between the predictive power of the different approaches, we simply report here different sets of fitting parameters.

Let us consider first the side-chain liquid crystal copolymer PMA80/20. We have recently shown[36] that the entropic model is able to describe satisfactorily the aging mechanism in this system. The considered experimental scans do not exhibit high overshooting peaks, so we put $w(i) = 1$ for each thermogram in eq 17. In Figure 2, the experimental scans selected among different thermal histories are shown together with the best fits obtained using the TNM model. The thermal histories pertaining to each measurement are reported on the figures. Appreciable discrepancies are observed between experimental and calculated traces, even if greater discrepancies were found in other systems in the literature.[21,37] The best fit parameters, obtained for different Δh settings, are reported in Table 1 together with the values of SS.

An inspection of Table 1 shows that similar values of SS are obtained for choices of the Δh parameter in a limited range of values. As expected, a comparable agreement between theory and experiments was found also by using the AGV model (eq 6). The best fit parameters found by the search routine for three

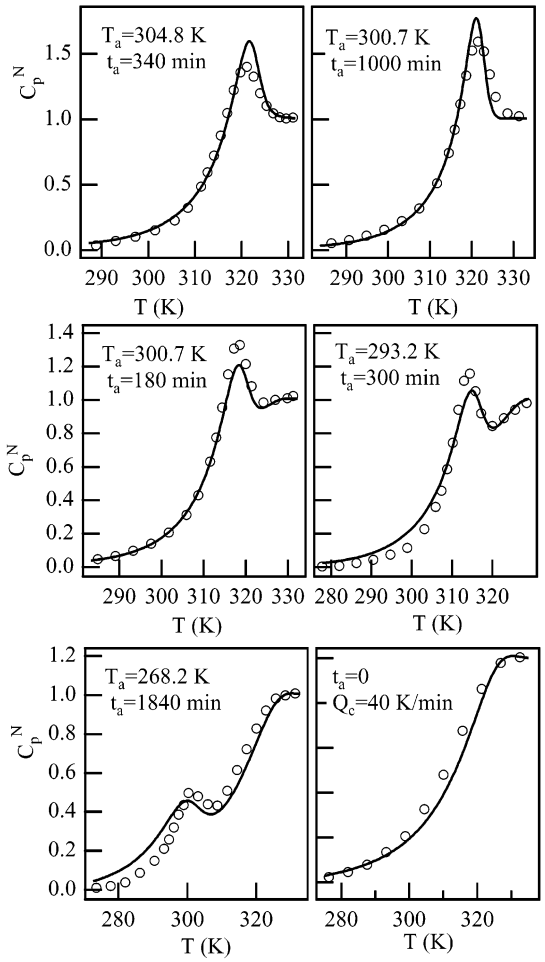

Figure 2. Simultaneous least-squares fit, obtained with the TNM model, of some DSC traces of PMA80/20 recorded after different thermal treatments. The aging temperatures and times are reported on the figures. $\Delta h/R = 54\ 126$ K; the other parameters are found in Table 1.

Table 1. Best Fit Parameters of the TNM Model in PMA80/20 for Different Choices of Δh

$\Delta h/R$ (K)	A (s)	x	β	SS
48 112	2.2×10^{-65}	0.39	0.27	0.0030
54 126	1.4×10^{-73}	0.30	0.26	0.0027
60 140	9.2×10^{-82}	0.24	0.24	0.0031

Table 2. Best Fit Parameters of the AGV Model in PMA80/20 for Different T_2 Settings

T_2 (K)	A (s)	B/R (K)	β	SS
237	1.2×10^{-16}	3156	0.26	0.0028
247	1.3×10^{-14}	2438	0.26	0.0026
257	1.8×10^{-12}	1793	0.25	0.0029

different values of the Adam−Gibbs temperature T_2 are reported in Table 2. It is seen that the best result, for $T_2 = 247$ K, provides a value SS = 0.0026 to be compared with the best value 0.0027 from the TNM model.

A remarkable improvement is found by fitting the same data with the configurational entropy model. In Figure 3, the best fits of this approach ($T_2 = 247$ K) are compared with the experimental scans already considered in Figure 2. It is apparent the better agreement of the theoretical prediction with each experimental trace. A more quantitative comparison is provided in Table 3, where the values of SS and the best fit parameters are reported for different choices of the Adam−Gibbs tem-

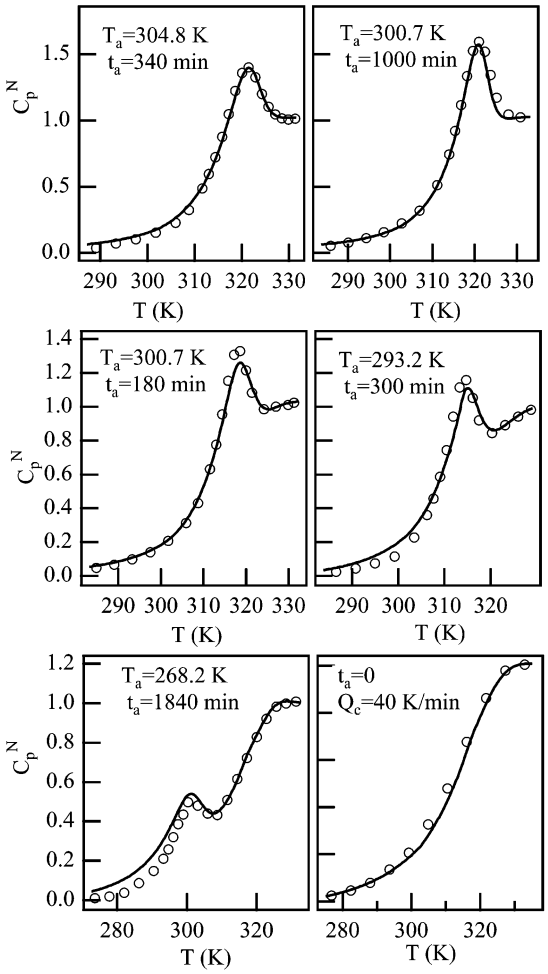

Figure 3. Comparison between the experimental scans of Figure 2 and the best fits provided by the configurational entropy approach developed by Gómez Ribelles and co-workers. $T_2 = 247$ K and the other parameters as in Table 3.

Table 3. Best Fit Parameters of the Configurational Entropy Model in PMA80/20 for Different T_2 Settings

T_2 (K)	A (s)	B (J/g)	δ (J/(g K))	β	SS
237	1.4×10^{-16}	1240	0.09	0.24	0.0018
247	5.3×10^{-14}	951	0.09	0.23	0.0018
257	8.4×10^{-13}	742	0.08	0.23	0.0020

perature. By inspection of Tables 1−3, it is seen that the average square error, SS, considerably decreases in the entropic approach with respect to TNM or AGV models. It is worth noting that the value of the additional parameter δ varies in the range 0.08−0.09 J/(g K), values corresponding to about 25% of the overall heat capacity change at the glass transition in this polymer ($\Delta C_p(T_g) \approx 0.34$ J/(g K)). As a consequence, the limit state at the end of structural relaxation turns out to be quite different from the one resulting from extrapolating the behavior in the melt.

A true evidence of this fundamental topic is not provided by the results shown in Figure 3 because one could argue that analogous improvement is obtainable from addition of one free parameter to TNM model. To gain further insight therefore we tempted to fit the data introducing the expressions discussed in section 2 (eqs 14−16). In Figure 4 the best fits found with eq 14 are superimposed to the experimental thermograms. The comparison between Figures 2 and 4 evidences the lack of a real improvement through eq 14. A quantitative comparison via SS (Table 4) supports this impression.

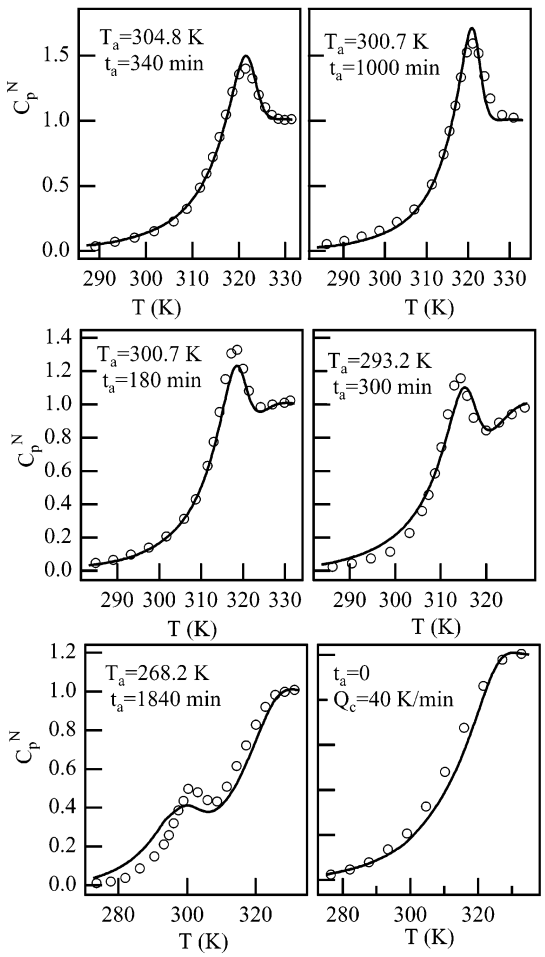

Figure 4. Comparison between the experimental scans of Figure 2 and the best fits provided by the TNM model modified with the quadratic correction (eq 14). $\Delta h/R = 54\,126$ K and the other parameters as in Table 4.

Table 4. Parameters of the TNM Model Modified with Eq 14, Obtained by the Search Routine in PMA80/20 for Different Δh Settings

$\Delta h/R$ (K)	A (s)	k (K^{-2})	x	β	SS
48 112	4.2×10^{-67}	2.7×10^{-3}	0.44	0.28	0.0026
54 126	2.6×10^{-75}	2.5×10^{-3}	0.34	0.26	0.0025
60 140	1.7×10^{-83}	2.4×10^{-3}	0.27	0.25	0.0029

Table 5. Parameters of the AGV Model Modified with Eq 15, Obtained by the Search Routine in PMA80/20 for Different T_2 Settings

T_2 (K)	A (s)	B/R (K)	m	β	SS
237	2.8×10^{-16}	3086	0.992	0.26	0.0026
247	4.1×10^{-14}	2351	0.988	0.26	0.0024
257	5.9×10^{-12}	1716	0.988	0.26	0.0026

Very similar results (pertinent figures are omitted) were found by using the power law dependence assumed in eq 15. In this case, as in the previous one, a small decrement of SS (see Table 5) was observed with respect to results obtained with the standard AGV expression. The values of the exponent m in fact were found to approach the unity for the different T_2 settings.

Finally, we tried to reproduce our data implementing the empirical relation of eq 16. The best fits obtained by setting $T_c = 257$ K are shown in Figure 5, whereas the different sets of parameters found by the search routine are reported in Table 6. Looking at the thermograms, it is seen that this expression, among the four

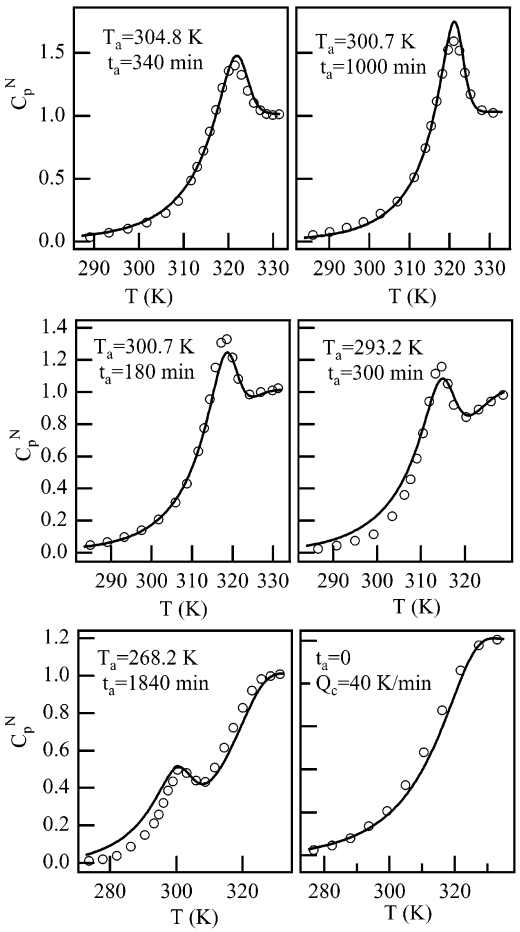

Figure 5. Comparison between the experimental scans of Figure 2 and the best fits provided by the approach defined by eq 16. $T_c = 257$ K, and the other parameters are reported in Table 6.

Table 6. Parameters of the Model Defined by Eq 16, Found by the Search Routine for PMA80/20 for Different T_c Settings

T_c (K)	A (s)	k	γ	β	SS
247	8.2×10^{-43}	57.8	33.2	0.27	0.0023
257	2.6×10^{-40}	52.4	28.6	0.27	0.0022
267	2.0×10^{-36}	44.3	24.3	0.26	0.0025

parameters relations, improves the agreement with some experimental scans, while the average square error SS appears to be larger than the one found with the configurational entropy approach. The collection of results provided by all the above models induces one to be more confident in the basic assumption of the entropic approach.

The same analysis was carried out for the PMMA polymer. Higher overshooting peaks were observed in its thermograms, so weighting factors $w(i)$ proportional to the inverse of the intensity of the overshooting peaks were assumed. It appears reasonable since it is well-known that thermal lag affects more seriously those measurements that provide higher overshooting peaks.[4] It should be remarked that the main results were not strongly dependent on this assumption, as we checked with some fitting procedures with $w(i) = 1$. In Figure 6, the selected experimental scans are shown together with the best fits obtained with the AGV model ($T_2 =$ 262 K) and the entropic approach ($T_2 = 282$ K). By inspection, it can be noted that the latter reduces the discrepancies in each single experimental thermogram

Table 7. Best Fit Parameters of the AGV Model for the PMMA Sample for Different T_2 Settings

T_2 (K)	A (s)	B/R (K)	β	SS
242	1.1×10^{-32}	11810	0.42	0.030
262	6.9×10^{-30}	9416	0.39	0.029
282	2.9×10^{-26}	7069	0.36	0.034
302	4.7×10^{-23}	5152	0.34	0.043
322	8.4×10^{-19}	3344	0.31	0.054
342	5.2×10^{-14}	1859	0.29	0.061

Table 8. Best Fit Parameters of the Configurational Entropy Model in PMMA for Different T_2 Settings

T_2 (K)	A (s)	B (J/g)	δ (J/(g K))	β	SS
262	9.9×10^{-30}	4113	0.069	0.40	0.015
282	7.0×10^{-27}	2967	0.076	0.37	0.014
302	1.5×10^{-23}	2018	0.085	0.35	0.017
322	1.3×10^{-19}	1249	0.091	0.32	0.022
342	7.6×10^{-15}	657	0.094	0.30	0.030

also in this sample. In Tables 7 and 8 the best fit parameters obtained at different T_2 temperatures are reported for the two models. The values of the SS column of these two tables, supporting quantitatively the above remarks, show that this parameter is now larger than in the previous sample. This is due to the values $w(i) > 1$ set for several scans and also to the higher peaks exhibited by the C_p^N curves.

In Figure 7, the same experimental scans are compared with the best fits from the TNM approach modified with the quadratic correction (eq 14). It can be seen, again, that such correction does not appreciably improve the agreement between experiments and theory despite the additional free parameter. Unsatisfactory results were also found from the modified AGV expression (eq 15). In the case of eq 14, the lowest square error was SS = 0.026 in correspondence of $\Delta h =$ 700 kJ/mol, to be compared with SS = 0.031 and SS = 0.029, the best results of TNM and AGV models, respectively, while adopting eq 15 the values of the exponent m ranged from 0.989 to 1.0008 depending on the T_2 setting.

As in studying the previous polymer, a more accurate description of the DSC thermograms were provided by the scaling expression of eq 16. The best results, corresponding to $T_c = 365$ K, are presented in Figure 8, while Table 9 reports the model parameters and the relative deviations SS for some T_c settings. It is confirmed that the results obtained with eq 16 are intermediate between those found by adopting the AGV and the configurational entropy approaches. The collection of the studies of the present work shows that the entropic model is the most suitable one to describe the DSC thermograms of the investigated polymer samples. The basic assumption of this model, according which the limit state attained at the end of structural relaxation is different from the one extrapolated from the melt, grows stronger. To gain more insight into its robustness, additional analysis can be carried out.

In Table 8, the mean value of $\delta \approx 0.08$ J/(g K) corresponds to about 30% of the overall heat capacity change at the glass transition ($\Delta C_p(T_g) \approx 0.29$ J/(g K)). Then the limit and the extrapolated state should result to be quite different: this should provide appreciable effects if experiments are performed after annealing procedures at long times, with the system approaching an equilibrium condition. A useful criterion to check the equilibrium of the glass is based on the well-known literature finding that the overshooting peaks observed

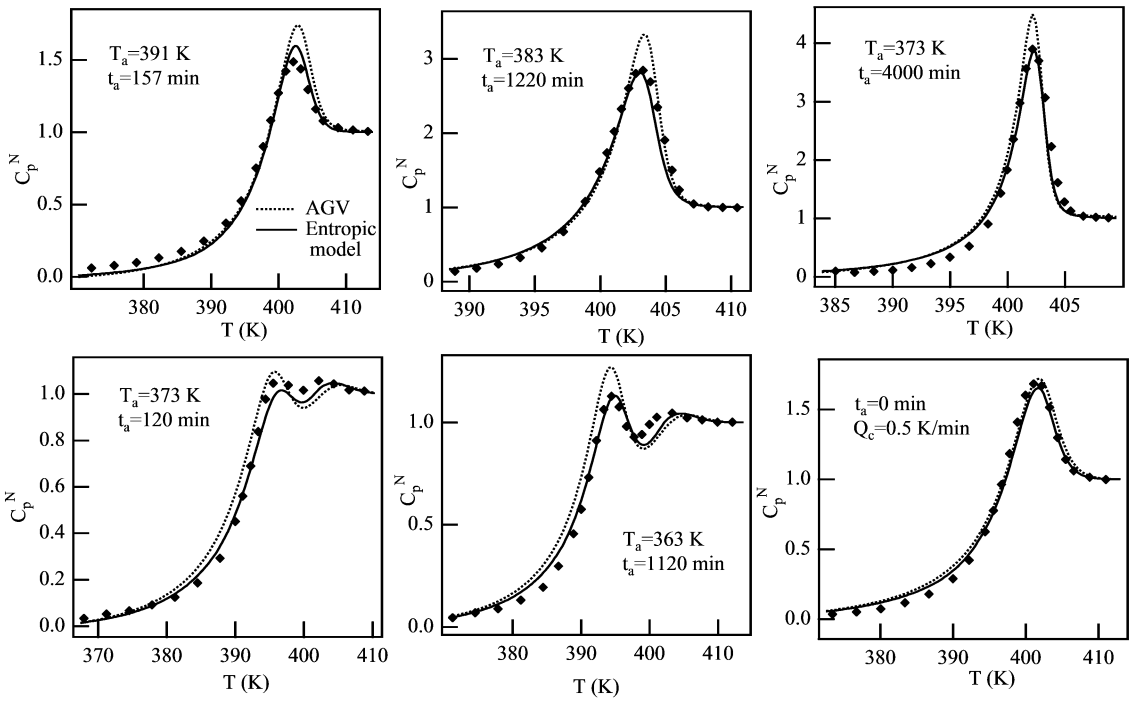

Figure 6. Simultaneous least-squares fit of six different DSC traces of PMMA obtained with the AGV and the configurational entropy model. The aging temperatures and times are reported on the figures. For the AGV model (dotted lines) $T_2 = 262$ K and the other parameters as in Table 7 whereas for the configurational entropy approach (continuous lines) $T_2 = 282$ K and the other parameters as in Table 8.

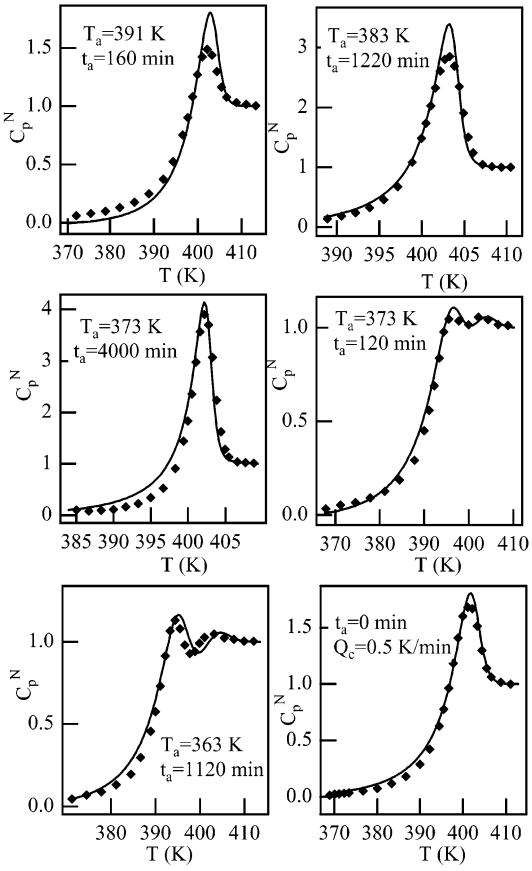

Figure 7. Comparison between the experimental scans of Figure 6 and the best fits provided by the TNM model modified with the quadratic correction (eq 14). $\Delta h = 700$ kJ/mol, $A = 1.3 \times 10^{-91}$ s, $x = 0.37$, $k = 1.08 \times 10^{-3}$, and $\beta = 0.39$.

in DSC traces after annealings at a constant glassy temperature shift toward higher temperatures as the annealing time is increased.[4]

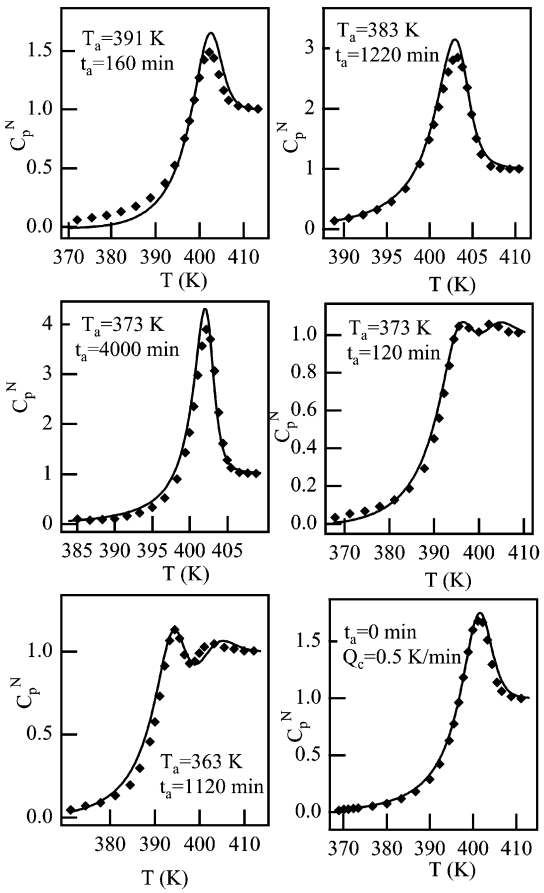

Figure 8. Comparison between the experimental scans of Figure 6 and the best fits provided by the TNM approach modified with eq 16. $T_c = 365$ K, and the other parameters are reported in Table 9.

In Figure 9, the temperatures corresponding to the maximum of the DSC overshooting peaks are reported

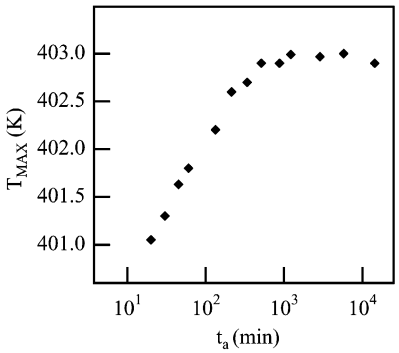

Figure 9. Dependence on annealing time of the temperature where the DSC peaks exhibit their maximum value for experiments carried out at $T_a = 388$ K.

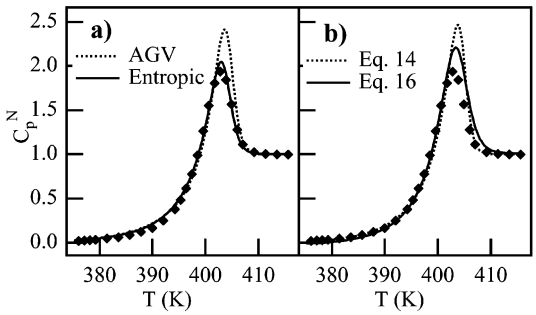

Figure 10. DSC thermogram recorded after annealing the PMMA sample for 1215 min at 388 K compared with the predictions of some of the multiparameter approaches analyzed in this work. The parameters are those providing the lowest square error in the simultaneous fitting procedure.

Table 9. Parameters of the Model Defined by Eq 16, Found by the Search Routine for the PMMA Sample

T_c (K)	A (s)	k	γ	β	SS
345	8.5×10^{-53}	72.4	26.5	0.39	0.029
355	1.4×10^{-51}	78.6	19.3	0.42	0.023
365	2.5×10^{-48}	78.4	13.9	0.44	0.022
375	9.1×10^{-43}	75.1	8.7	0.45	0.028

as a function of the annealing time for experiments carried out on PMMA at $T_a = 388$ K, about 4 K below T_g. From the T_{max} behavior it is concluded that the system is at its steady state for $t_a > 1000$ min. In Figure 10a, the experimental normalized heat capacity curve of the PMMA sample with annealing thermal history $t_a = 1215$ min, $T_a = 388$ K is shown together with the best prediction of the AGV and configurational entropy models. Figure 10b shows the comparison for the modifications of TNM and AGV models defined by eqs 14 and 16, respectively. By inspection, the experimental data are better reproduced by the configurational entropy approach, confirming its robustness. In fact, the area enclosed below the DSC overshooting peak is related to the value of the enthalpy lost during the annealing step,[4,39] and the overestimation of the maximum amount of releasable enthalpy with TNM or AGV models means that the limit state has a configurational enthalpy (and entropy) higher than the extrapolated state, just as stated by the entropic approach. The analysis of the enthalpy loss on aging at $T_a = 388$ K provides a further check of the robustness of the entropic model.

According to the literature, the enthalpy lost on aging a glass is evaluated by the expression

$$\Delta H(T_a,t_a) = \int_{T_x}^{T_y} [C_p^a(T) - C_p^u(T)]\, dT \qquad (18)$$

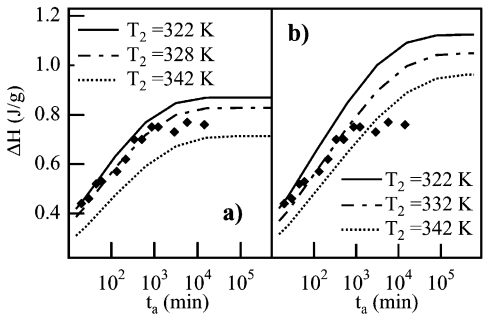

Figure 11. Enthalpy lost on aging the PMMA sample at 388 K as a function of the annealing time. The symbols are experimental data evaluated from eq 18. (a) The lines are the predictions of the configurational entropy approach for some different T_2 settings. For $T_2 = 328$ K, $A = 3.3 \times 10^{-18}$ s, $B = 1050$ J/g, $\delta = 0.088$, and $\beta = 0.31$; parameters concerning other T_2 values are given in Table 8. (b) The lines are the predictions of the AGV model for different T_2 settings (other parameters in Table 7).

with $C_p^a(T)$ and $C_p^u(T)$ the heat capacity after annealing at T_a for the time t_a and the heat capacity of the unannealed sample, respectively. T_x and T_y are reference temperatures ($T_x < T_g < T_y$) where the two signals overlap. This relation, to be precise, provides the enthalpy difference between the two thermal histories (with and without the annealing step) at that temperature where the second cooling stops and the subsequent heating starts (T_s). Therefore, it represents an approximation by defect of the enthalpy change during the annealing step, which becomes very precise at T_a low enough.[39,40] However, the comparison between the experimental results evaluated according to eq 18 and the correspondent theoretical predictions might provide additional information concerning the effective ability of the different models in describing the structural relaxation.

In Figure 11a, the $\Delta H(T_a,t_a)$ values evaluated according to eq 18 and pertaining to the experiments carried out at $T_a = 388$ K are compared with the theoretical predictions of the configurational entropy model for some different T_2 settings (other parameters in Table 8 and in the figure caption). In fact, in this work it has been found that the calculated values of the enthalpy lost $\Delta H(T_a,t_a)$ on aging the sample, or more precisely the enthalpy difference at the starting scan temperature, remarkably depend on the T_2 settings. Similar conclusions have been reached recently for the AGV model.[41] In Figure 11a, the experimental data are bounded by the two theoretical curves pertaining to the extreme T_2 settings. In particular, by averaging the data pertaining to $t_a > 1000$ min, we found $\Delta H_\infty^{exp}(388\text{ K}) = 0.75$ J/(g K) to be compared with the calculated values $\Delta H_\infty^{entropic}(T_2 = 322\text{ K}) = 0.86$ J/(g K) and $\Delta H_\infty^{entropic}(T_2 = 342\text{ K}) = 0.71$ J/(g K), respectively. Note that, looking at the model results that provide the best agreement at short times ($T_2 = 328$ K), the entropic model only slightly overestimates the asymptotic experimental value, which could be due to a little underestimation of the δ parameter by the search routine. The same analysis carried out for the AGV model is shown in Figure 11b. In this case the results are very different because only at short times the experimental data are bounded by the two extreme theoretical predictions, being the limit asymptotic values greatly overestimated by the model ($\Delta H_\infty^{AGV}(T_2 = 342\text{ K}) = 0.96$ J/(g K) and $\Delta H_\infty^{AGV}(T_2 = 322\text{ K}) = 1.12$ J/(g K)). The TNM extended

models, which also assume the extrapolation procedure in order to define the equilibrated limit state, exhibited similar behavior. The same analysis was carried out for experiments at $T_a = 382$ K; however, the conclusions appear to be blurred by the failure of the system to reach the equilibrium in the time window accessed by our measurements.

5. Conclusion

In this work the ability of multiparameter models on describing the aging mechanism of polymers has been analyzed. The TNM or AGV models, able to give account of the main features of the aging mechanism, often find difficulties in describing quantitatively DSC experiments. One possible reason for these difficulties originates from handling of nonlinearity through the expression relating the instantaneous relaxation times to the temperature and the structure of the glass. A few years ago, Gómez Ribelles and co-workers proposed a configurational entropy approach which improves the predictive power in several polymers with respect to TNM or AGV models. However, this model introduces an additional free parameter and modifies one of the fundamental assumptions of TNM formalism according to which the long-term equilibrated values of thermodynamic variables in the glass are obtained by extrapolating the melt behavior. To investigate this important topic, we compared DSC experiments performed in two different polymers with the predictions of the entropic approach and other possible extensions of the TNM formalism. In this second group of models the original treatment of nonlinear effects was modified by adding a free fitting parameter while maintaining the basic assumption of TNM model.

For both the polymers here considered, the entropic approach was found to give the best agreement with the DSC thermograms. Furthermore, the experiments performed after long times annealing in the glass, with the system approaching the equilibrium, seem to support the assumption of the entropic model while providing a further discriminating criterion to single out the best set of material parameter. In fact, the limit value of the enthalpy lost on aging the glass results to be in good agreement with the prediction of the entropic approach at variance with the other approaches which overestimated it at a greater extent. The collection of the tools developed to analyze the experimental thermograms, which may be summarized as simultaneous best fitting of different thermal histories of the material, evaluation of the square deviation (eq 17) and analysis of the enthalpy lost at long annealing times not only allows one to select the most suitable model and material parameter set but also, interestingly enough, singles out among the others just the parameters set that exhibits meaningful values of the prefactors A and the $T_g - T_2$ difference. The results presented in this work dealing with a fundamental issue of the glassy state appear a stimulating starting point for further investigation, to be carried out for a wider variety of polymeric systems and annealing temperatures.

Acknowledgment. This work is supported by the MIUR and INFM (CIPE project P5BW5).

References and Notes

(1) Struick, L. C. E. *Physical Aging in Amorphous Polymers and Other Materials*; Elsevier: New York, 1978.
(2) Hutchinson, J. M. *Prog. Polym. Sci.* **1995**, *20*, 703−760.
(3) Alegría, A.; Goitiandía, L.; Tellería, I.; Colmenero, J. *Macromolecules* **1997**, *30*, 3881−3887.
(4) Hodge, I. M. *J. Non-Cryst. Solids* **1994**, *169*, 211−267.
(5) McKenna, G. B.; Simon, S. L. In *Time Dependent and Nonlinear Effects in Polymers and Composites*; Schapery, R. A., Sun, C. T., Eds.; American Society for Testing and Materials: West Conshohocken, PA, 2000; pp 18−46.
(6) Drozdov, A. D. *Phys. Lett. A* **1999**, *258*, 158−170.
(7) Drozdov, A. D. *J. Polym. Sci., Part B: Polym. Phys.* **2001**, *39*, 1312−1325.
(8) Gutzow, I.; Llieva, D.; Babalievski, F.; Yamakov, V. *J. Chem. Phys.* **2000**, *112*, 10941−10948.
(9) Narayanaswamy, O. S. *J. Am. Ceram. Soc.* **1971**, *54*, 491−498.
(10) Moynihan, C. T.; Easteal, A. J.; Tran, D. C.; Wilder, J. A.; Donovan, E. P. *J. Am. Ceram. Soc.* **1976**, *59*, 137−140.
(11) DeBolt, M. A.; Easteal, A. J.; Macedo, P. B.; Moynihan, C. T. *J. Am. Ceram. Soc.* **1976**, *59*, 16−21.
(12) Tool, A. Q. *J. Am. Ceram. Soc.* **1946**, *29*, 240−253.
(13) Tribone, J. J.; O'Reilly, J. M.; Greener, J. *Macromolecules* **1986**, *19*, 1732−1739.
(14) Cowie, J. M. G.; Ferguson, R. *Polymer* **1993**, *34*, 2135−2141.
(15) Cowie, J. M. G.; Harris, S.; McEwen, I. J. *J. Polym. Sci., Part B: Polym. Phys.* **1997**, *35*, 1107−1116.
(16) Simon, S. L. *Macromolecules* **1997**, *30*, 4056−4063.
(17) O'Reilly, J. M.; Hodge, I. M. *J. Non-Cryst. Solids* **1991**, *131−133*, 451−456.
(18) Moynihan, C. T.; Crichton, S. N.; Opalka, S. M. *J. Non-Cryst. Solids* **1991**, *131−133*, 420−434.
(19) Gómez Ribelles, J. L.; Monleón Pradas, M. *Macromolecules* **1995**, *28*, 5867−5877.
(20) Meseguer Dueñas, J. M.; Garayo, A. V.; Romero Colomer, F.; Estellés, J. M.; Gómez Ribelles, J. L.; Monleón Pradas, M. *J. Polym. Sci., Part B: Polym. Phys.* **1997**, *35*, 2201−2217.
(21) Gómez Ribelles, J. L.; Monleón Pradas, M.; Garayo, A. V.; Romero Colomer, F.; Estellés, J. M.; Meseguer Dueñas, J. M. *Polymer* **1997**, *38*, 963−969.
(22) Scherer, G. W. *J. Am. Ceram. Soc.* **1984**, *67*, 504−511.
(23) Hodge, I. M. *Macromolecules* **1987**, *20*, 2897−2908.
(24) Adam, G.; Gibbs, J. H. *J. Chem. Phys.* **1965**, *43*, 139−146.
(25) Hodge, I. M. *J. Res. Natl. Inst. Stand. Technol.* **1997**, *102*, 195−205.
(26) Kauzmann, W. *Chem. Rev.* **1948**, *43*, 219−256.
(27) Gómez Ribelles, J. L.; Monleón Pradas, M.; Meseguer Dueñas, J. M.; Privalko, V. P. *J. Non-Cryst. Solids* **1999**, *244*, 172−184.
(28) Málek, J.; Montserrat, S. *Thermochim. Acta* **1998**, *313*, 191−200.
(29) Málek, J. *Macromolecules* **1998**, *31*, 8312−8322.
(30) Colby, R. H. *Phys. Rev. E* **2000**, *61*, 1783−1792.
(31) Götze, W.; Sjögren, L. *Rep. Prog. Phys.* **1992**, *55*, 241−376.
(32) Angeloni, A. S.; Caretti, D.; Laus, M.; Chiellini, E.; Galli, G. *J. Polym. Sci., Polym. Chem. Ed.* **1991**, *29*, 1865−1873.
(33) Richardson, M. J.; Savill, N. G. *Polymer* **1975**, *16*, 753−757.
(34) Nedler, J. A.; Mead, R. *Comput. J.* **1965**, *7*, 308.
(35) Hodge, I. M.; Berens, A. R. *Macromolecules* **1982**, *15*, 762−770.
(36) Andreozzi, L.; Faetti, M.; Giordano, M.; Palazzuoli, D. *Macromolecules* **2002**, *35*, 6049−9056.
(37) See the case of PMMA in: Hodge, I. M. *Macromolecules* **1983**, *16*, 898−902.
(38) Cowie, J. M. G.; Ferguson, R. *Macromolecules* **1989**, *22*, 2307−2312.
(39) Gómez Ribelles, J. L.; Ribes Greus, A.; Díaz Calleja, R. *Polymer* **1990**, *31*, 223−230.
(40) Andreozzi, L.; Faetti, M.; Giordano, M.; Palazzuoli, D., submitted to *J. Non-Cryst. Solids.*
(41) Andreozzi, L.; Faetti, M.; Giordano, M.; Palazzuoli, D. *J. Phys.: Condens. Matter* **2003**, *15*, S1215−S1226.

MA0347870